ACS NANO

www.acsnano.org

ARTICLE

Pomegranate-Structured Conversion-Reaction Cathode with a Built-in Li Source for High-Energy Li-Ion Batteries

Xiulin Fan,[†] Yujie Zhu,[†] Chao Luo,[†] Liumin Suo,[†] Yan Lin,[†] Tao Gao,[†] Kang Xu,[*,‡] and Chunsheng Wang[*,†]

[†]Department of Chemical and Biomolecular Engineering, University of Maryland, College Park, Maryland 20742, United States

[‡]Electrochemistry Branch, Power and Energy Division Sensor and Electron Devices Directorate, U.S. Army Research Laboratory, Adelphi, Maryland 20783, United States

Supporting Information

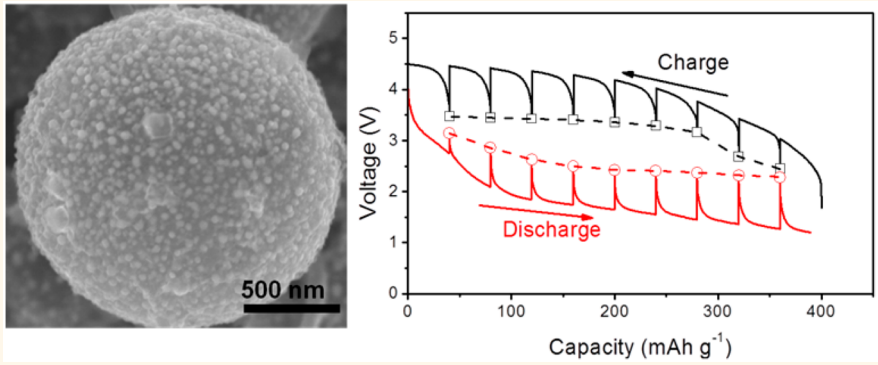

ABSTRACT: Transition metal fluorides (such as FeF_3 or CoF_2) promise significantly higher theoretical capacities (>571 mAh g^{-1}) than the cathode materials currently used in Li-ion batteries. However, their practical application faces major challenges that include poor electrochemical reversibility induced by the repeated bond-breaking and formation and the accompanied volume changes and the difficulty of building an internal Li source within the material so that a full Li-ion cell could be assembled at a discharged state without inducing further technical risk and cost issues. In this work, we effectively addressed these challenges by designing and synthesizing, *via* an aerosol-spray pyrolysis technique, a pomegranate-structured nanocomposite FeM/LiF/C (M = Co, Ni), in which 2−3 nm carbon-coated FeM nanoparticles (~10 nm in diameter) and LiF nanoparticles (~20 nm) are uniformly embedded in a porous carbon sphere matrix (100−1000 nm). This uniquely architectured nanocomposite was made possible by the extremely short pyrolysis time (~1 s) and carbon coating in a high-temperature furnace, which prevented the overgrowth of FeM and LiF in the primordial droplet that serves as the carbon source. The presence of Ni or Co in FeM/LiF/C effectively suppresses the formation of Fe_3C and further reduces the metallic particle size. The pomegranate architecture ensures the intimate contact among FeM, LiF, and C, thus significantly enhancing the conversion-reaction kinetics, while the nanopores inside the pomegranate-like carbon matrix, left by solvent evaporation during the pyrolysis, effectively accommodate the volume change of FeM/LiF during charge/discharge. Thus, the FeM/LiF/C nanocomposite shows a high specific capacity of >300 mAh g^{-1} for more than 100 charge/discharge cycles, which is one of the best performances among all of the prelithiated metal fluoride cathodes ever reported. The pomegranate-structured FeM/LiF/C with its built-in Li source provides an inspiration to the practical application of conversion-reaction-type chemistries as next-generation cathode materials for high-energy density Li-ion batteries.

KEYWORDS: *conversion-reaction cathode materials, prelithiation, transition metal fluorides, FeF_3*

After more than two decades of optimization, the energy density of the state-of-the-art Li-ion batteries (LIBs) approaches the upper limits imposed by the intercalation chemistries of their cathode materials, where typically less than one Li could be stored by each transition metal

Received: April 5, 2016
Accepted: May 10, 2016
Published: May 10, 2016

DOI: 10.1021/acsnano.6b02309
ACS Nano 2016, 10, 5567−5577

core.[1−3] Beyond the horizon of LIBs, there are a number of chemistries that promise superior capacities and energy densities, each of which, however, comes with severe challenges to overcome before their practical applications become a reality.[4] In particular, with the relatively more successful development of alloy-type anode materials, the need for cathode materials with comparably high capacity becomes ever more needed.[5,6]

Recently, intensive efforts have been dedicated to such cathode chemistries that involve conversion reaction instead of intercalation mechanisms, examples of which includes sulfur-based as well as transition metal fluorides.[7−13] They break out the capacity limits set by the intercalation mechanism by accommodating more than one Li^+ per equivalence of active core, generating transition metal (TM) and Li_2S or LiF phases during discharge and re-forming the original TM_aX_b (X = S, F) phases upon charging:

$$TM_aX_b + nbLi^+ + ne \leftrightarrow bLi_nX + aTM \quad (1)$$

Among these candidates, transition metal fluorides were considered the most promising due to their higher electrochemical potentials,[14,15] which resulted from the higher ionicity of TM−F bonds compared to that of their metal sulfide counterparts. Among TM−F cathodes, FeF_3 exhibits the highest theoretical capacity of 712 mAh g^{-1} (assuming a complete $3e^-$ reaction) at an average potential of ∼2.74 V,[14] alluding to a high theoretical energy density of 1950 Wh kg^{-1}.[16] However, their commercialization, like any conversion-reaction chemistry, is still prevented by the following major hurdles:[16] (1) the huge potential hysteresis between the lithiation/delithiation process[18,19] induced by the low ionic/electronic conductivity and the large band gap of the TM fluorides;[17,18] this disadvantage would be further deteriorated by the slow phase transition kinetics that involves the repeated breaking and re-formation of TM−F bonds in each electrochemical cycle; (2) the rapid capacity fading as the cycling proceeds that is induced by mechanical strain due to a 41−57% volume expansion upon discharging (lithiation) and the consequent pulverization of these materials, as well as the gradual overgrowth of transition metal clusters during cycling.

In order to address these two challenges, various nanostructures constructed by high-energy ball-milling,[20] HF-based aqueous solution synthesis,[21,22] solid−liquid reaction,[10] ion liquid synthesis method,[23−25] and physical vapor deposition[26,27] were introduced in the hope that reaction kinetics would be accelerated due to shortened electron and ion diffusion distances, and that pulverizations due to volume expansion would be relieved by nanosized domains. Impressive advances have indeed ensued,[10,28] but the life of conversion-reaction cathodes is still typically characterized by fast capacity decay in less than 20 cycles, accompanied by extremely poor kinetics.[10,28,29] The third challenge, little attended thus far but nonetheless critical to commercial production, is the absence of a built-in Li source in these conversion-reaction materials. The consequent implication is that these nonlithiated materials, if successful, can only be assembled into a cell at a fully charged state against a prelithiated anode, which is not available in the LIB industry and would induce further risks and costs.[30,31]

Efforts have been made to design a prelithiated version of transition metal fluorides,[32−36] but their electrochemical performances are far worse when compared to their non-lithiated counterparts as characterized by either lower capacity utilization (<180 mA h g^{-1}),[33−35] shorter cycle life (∼20 cycles),[35,36] or even higher hysteresis,[33,35,36] which might be due to the unfavorable distribution of transition metal and LiF species, the poor contact among all active components, and the intrinsically insulating nature of relatively large LiF particles. The reason for much better reversibility of the nonlithiated TM fluorides might come from the *in situ* formation of extremely small LiF and TM particles that are evenly mixed with each other during the first discharge (lithiation) process.[37−40] It was estimated that, in order to achieve effective utilization of Fe in lithiated FeF_3 through the conversion reaction, Fe particle size should be less than 20 nm,[28,41] which remains difficult to obtain *via* conventional synthesis technologies.

In the present work, we developed a facile and scalable one-step aerosol-spray pyrolysis approach to synthesize a prelithiated nanocomposite consisting of ternary components of FeM (M = Ni, Co), LiF, and C, in which the two active ingredients, FeCo or FeNi nanoparticles (∼10 nm) and LiF nanoparticles (∼20 nm) that were formed *in situ* during the flight through the pyrolysis tube, are evenly distributed throughout a porous graphitic carbon sphere. FeF_3 was selected as the model cathode due to its high theoretical capacity, nontoxicity, low cost, and high natural abundance. The resultant pomegranate-like nanostructure ensures the intimate contact between the active species (FeM and LiF) and the carbonaceous conductive agent. Meanwhile, the flexible and conductive 3D carbonaceous matrix can effectively absorb the mechanical stress induced by the volume change while inhibiting possible aggregation of FeM, thus maintaining the structural and electrical integrity of the nanocomposite during the repeated chemical bond formation and breaking cycles.

As an example, the prelithiated FeCo/LiF/C nanocomposites can deliver a stable capacity of over 300 mAh g^{-1} (based on the total mass of FeCo/LiF/C) for more than 100 cycles in the voltage range of 1.2−4.5 V at room temperature, exhibiting the best of the prelithiated TM fluorides reported to date while demonstrating much higher capacity than the conventional intercalation cathode. The pomegranate-like nanostructure readily achieved *via* the aerosol-spray pyrolysis approach opens up opportunities in the exploration of conversion-reaction-type chemistries for high-performance next-generation LIBs.

RESULTS AND DISCUSSION

Material Preparation and Characterization. The formation of nanospheres of composite FeM/LiF/C (M = Co, Ni) is attributed to the extremely short residential flight time (∼1.0 s) of primordial droplets through the pyrolysis furnace in the aerosol-spray process, which leads to a pomegranate-like structure that integrates nano-FeM and nano-LiF within a microcarbon sphere, as shown schematically in Figure 1.

Detailed procedures are described in the Experimental Section. In brief, the transparent precursor solution is atomized into microsized droplets and then swept by an Ar/H_2 carrier gas into a 750 °C furnace with shorter than 1 s exposure to pyrolysis. Each primordial droplet, 100−1000 nm in diameter, serves as a microreactor in the reductive atmosphere and experiences a quick heating and cooling process before the eventual formation of a ternary composite, which, inheriting the physical shape of precursor droplets, are spheres of 100−1000 nm in diameter. The main advantage of such a technique is that single- or multicomponent particles can be formed rapidly in a single step with each particle generated from an individual

DOI: 10.1021/acsnano.6b02309
ACS Nano 2016, 10, 5567−5577

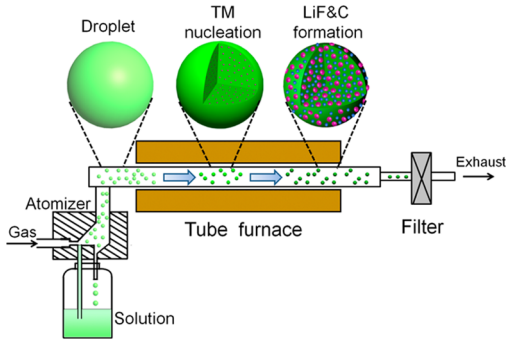

Figure 1. Schematic illustration for the fabrication of TM (TM = FeCo, FeNi)/LiF/C nanocomposite cathode materials with pomegranate-like nanoarchitecture.

droplet. The sphere sizes of FeM/LiF/C and the primary FeM and LiF particle sizes in the pomegranate can be easily manipulated by changing the atomizer powers, furnace temperatures, precursor solution concentrations, and carrier gas flow rates.

The key to the formation of the above pomegranate-like nanoarchitecture is rooted in the instantaneous heating of microsized precursor droplets, where nanograins of FeM and LiF are rapidly generated from solution under high temperature and reductive environment, while at the same time, the sucrose-containing solution rapidly carbonizes into a thin carbonaceous coating on the nascent FeM nanograins due to high catalytic activity of transition metal for carbon formation.[42] This *in situ* formed carbon coating prevents the overgrowth of FeM nanoparticles and quickly merges with each other and encapsulates FeM and LiF nanoparticles together inside the spherical carbon matrix, forming a porous carbonaceous sphere evenly embedded with individual FeM and LiF nanograins, in close resemblance to distinct seeds distributed within a pomegranate. The primordial droplet size (<1 μm) defines the pomegranate size, while the concentration and pyrolysis/cooling rate (a few seconds) controls the FeM and LiF nanoparticle size. Such an arrangement of active species within a porous carbonaceous sphere at such short lengths is especially important for the metal fluoride materials since the conversion reaction involves not only the transport of Li but also the diffusion of the heavier ion of F^- during the charge and discharge processes.

Figure 2a shows the X-ray diffraction (XRD) patterns of as-synthesized Fe/LiF/C, FeCo/LiF/C, and FeNi/LiF/C materials. In the Fe/LiF/C composite, Fe_3C is formed in an appreciable amount due to the reaction between the *in situ* formed Fe nanoparticles and carbon at the high temperature. Fe_3C was also observed in the conventional pyrolysis of Fe and carbon composite materials.[43,44] Since the Fe_3C is inactive to electrochemical lithiation,[45] the formation of the Fe_3C significantly reduces the capacity of the Fe/LiF/C composite. In contrast, no diffraction peaks corresponding to Fe_3C and other carbide phases are detected in FeCo/LiF/C and FeNi/LiF/C nanocomposites, demonstrating that Fe alloying with Co or Ni effectively prevents Fe_3C formation during pyrolysis, probably because the formation enthalpies of Ni and Co carbides are much larger than that of Fe_3C,[46,47] while alloying of Fe with Co or Ni increases the formation enthalpy of Fe_3C. Only the FeCo (PDF# 65-4131) or FeNi (PDF# 47-1417) and LiF (PDF# 45-1460) phases are detected for the FeM/LiF/C nanocomposites. Because most of the FeCo diffraction peaks

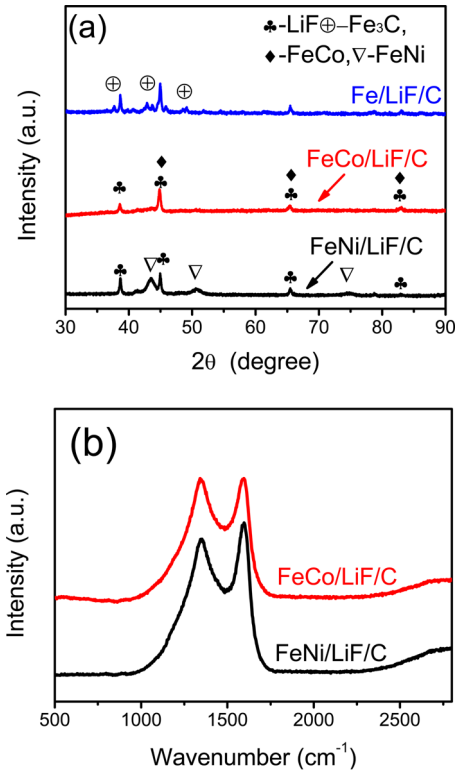

Figure 2. XRD patterns and Raman spectra for the as-synthesized Fe/LiF/C, FeCo/LiF/C, and FeNi/LiF/C composites.

overlap with those of LiF, it is difficult to detect the presence of FeCo in FeCo/LiF/C composite. However, FeNi sufficiently differs from LiF (Figure 2a), thus allowing us to characterize FeNi and LiF phases. The average crystal sizes of FeNi and LiF calculated from their largest diffraction peaks using Scherrer's equation are about 7.2 and 19.8 nm, respectively. The smaller size of FeNi nanoparticles compared to LiF might be attributed to the instantaneous carbon coating on nascent FeNi cores due to the high catalytic activity of FeNi for carbonization, which suppresses its sustained growth.[42] Due to the short residence time, it is expected that coated carbon on the FeNi nanoparticle core is only partially graphitized with few graphene layers, thus both Li^+ and F^- can rapidly diffuse through graphene during the conversion reaction. Raman spectra for the FeCo/LiF/C and FeNi/LiF/C in Figure 2b show two broad peaks at about 1345 and 1595 cm^{-1}, respectively, confirming the coexistence of disordered graphite (D band) and crystalline graphite (G band).

The composition of the FeCo/LiF/C nanocomposite was determined using thermogravimetric analysis (TGA) at a heating rate of 3 °C/min in air (Supporting Information Figure S1). Almost no weight change was observed from 100 to 200 °C, indicating that there is no Fe/Co or carbon oxidation below 200 °C. The weight increase from 200 to 275 °C is attributed to the oxidation of metallic Fe and Co, while the subsequent weight loss from 280 to 400 °C is mainly due to the carbon oxidation, releasing CO_2. If it is assumed that the final products are Fe_2O_3, Co_3O_4, and LiF after TGA measurement, the content of active species (FeCo and LiF) in the composite is determined to be 65 wt %.

SEM images of the FeCo/LiF/C composite (Figure 3a–c) reveal primary FeCo and LiF nanoparticles (10–20 nm in diameter) evenly scattered within the microsized secondary

DOI: 10.1021/acsnano.6b02309
ACS Nano 2016, 10, 5567–5577

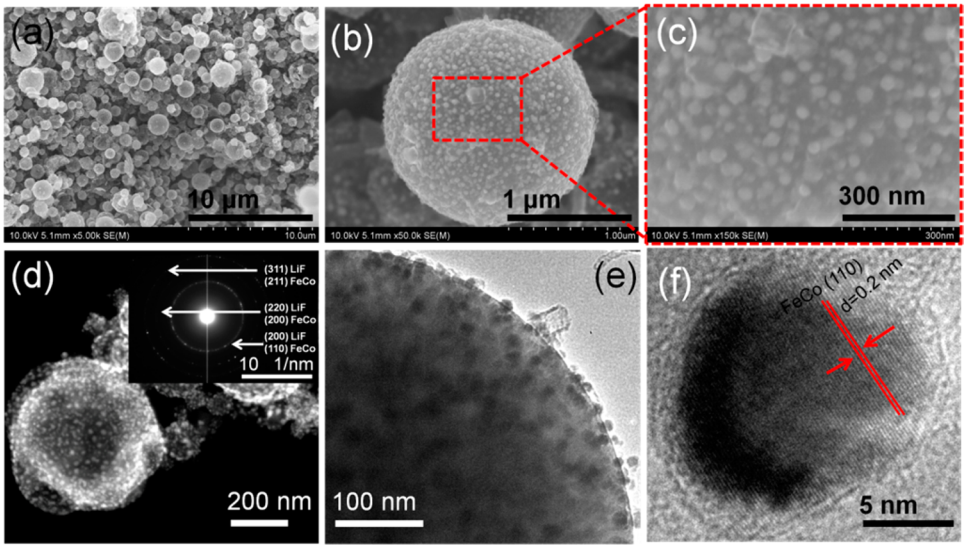

Figure 3. Microscopic images of as-synthesized FeCo/LiF/C nanocomposites: (a–c) SEM images; (d) HAADF-STEM image, with the inset being the corresponding SAED patterns; (e) TEM image; and (f) HRTEM image of the dark nanoparticle in (e).

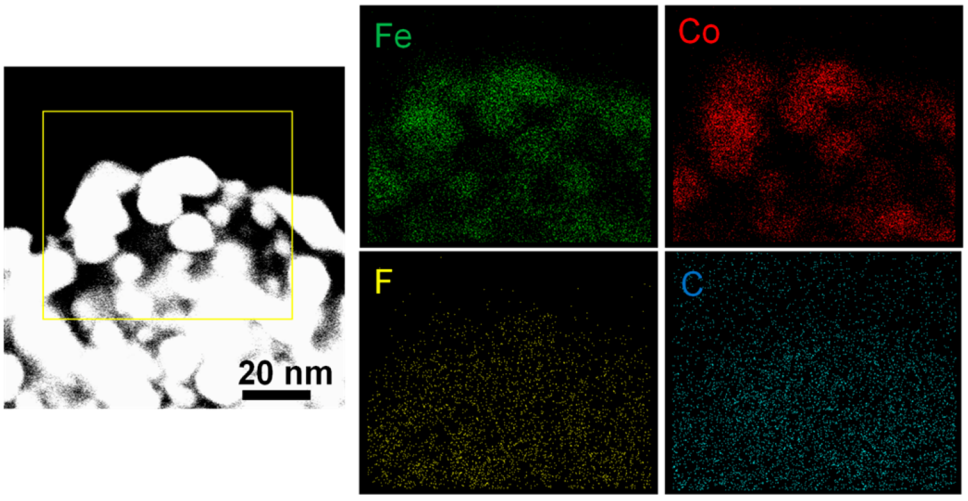

Figure 4. HAADF-STEM image of an as-synthesized FeCo/LiF/C composite and the corresponding EDS mapping of Fe, Co, F, and C. The rectangle in the image denotes the EDS mapping area.

carbon spherical particles, with a number of nanoparticles protruding out of the surface of the secondary carbon spherical particles, resembling a pomegranate in architecture. Figure 3d shows the STEM-HAADF (scanning transmission electron microscopy high-angle annular dark-field) image of the composite. Since the intensity of STEM-HAADF is proportional to $z^{1.7}$ (z is the atomic number), the elements with different atomic numbers can be clearly observed in the STEM-HAADF mode, where the brighter color represents the heavy elements (Fe and Co), and the dark region represents C/LiF composites. STEM image in Figure 3d and selected area electron diffraction (SAED) patterns (inset in Figure 3d) confirm that the FeCo and LiF nanoparticles are embedded in carbon sphere particles. The diffuse rings of SAED patterns indicate that the crystalline sizes of FeCo and LiF are very small, in accordance with the broad peaks of XRD patterns. TEM images (Figure 3e) further confirm that the distribution of primary FeCo nanoparticles continues throughout the interior of secondary carbon spheres. High-resolution (HR) TEM (Figure 3f) identified thin layers of carbon (2–3 nm thickness) surrounding FeCo cores, where the dark crystal region represents FeCo and the light region is C/LiF composites. Few-layer nanographene encapsulation (<6 stacked layers, ~2 nm) could be observed on almost every FeCo nanoparticle (see Figure S2 for more HRTEM images), which is in line with the crystalline graphite (G band) in the Raman spectra (Figure 2b). The FeCo nanoparticle in Figure 3f shows that the single-crystal structure and the lattice fringes of ~0.2 nm correspond to the (110) planes of the FeCo cubic structure.

The TEM image and corresponding element mappings with EDS (Figures 4) reveal that F and C elements are homogeneously mixed within the spheres, which strongly implies that LiF is integrated into a carbon composite matrix, while the overlap of Fe and Co mapping confirms the alloying between Fe and Co, while the FeCo nanocrystallites are evenly dispersed in the vicinities of LiF and carbon; therefore, intimate contacts among all four subcomponents are expected. In summary, the nanocomposite bears close resemblance to the hierarchy of a pomegranate, where the primary transition metal FeCo nanoparticles are evenly embedded in the matrix of C

DOI: 10.1021/acsnano.6b02309
ACS Nano 2016, 10, 5567–5577

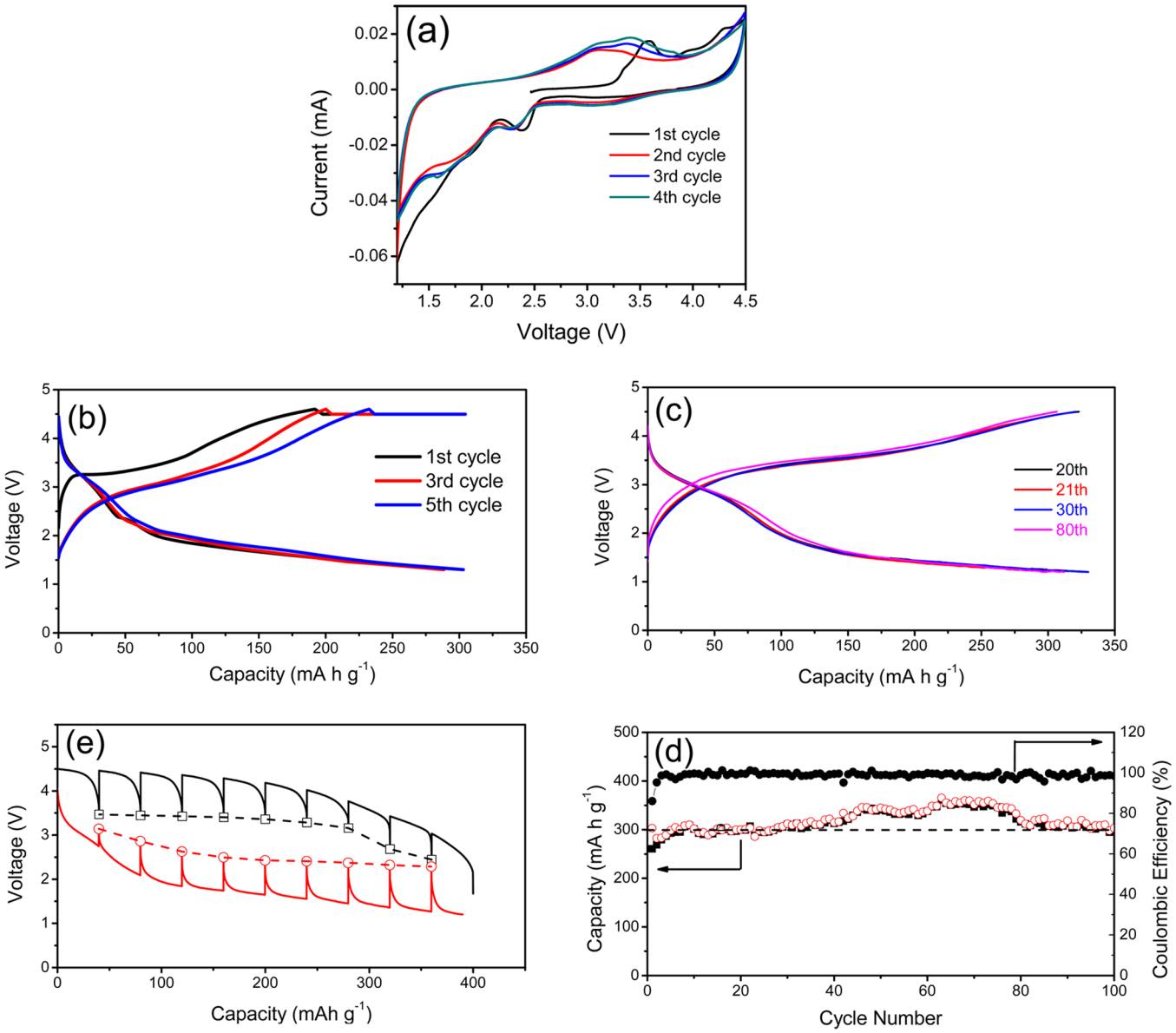

Figure 5. Electrochemical performances of the nanocomposite cathode material with pomegranate architecture: (a) Cyclic voltammograms of the initial four cycles scanned between 1.2 and 4.5 V at a rate of 0.1 mV/s; (b) representative activation charge/discharge profiles in the first five cycles; (c) representative charge/discharge curves for different cycles; (d) cycling performance at 1.2−4.5 V and 30 mA/g; (e) quasi-equilibrium voltage profile obtained from galvanostatic intermittent titration technique measurements (40 mA g^{-1} for 1 h followed by a 20 h rest). All measurements were performed at room temperature.

and LiF, while all active components are well-connected by conducting pathways.

The porous structure of the FeCo/LiF/C composite was determined by N_2 isothermal adsorption−desorption measurement using the Barrett−Joyner−Halenda model. Figure S3 depicts the N_2 adsorption−desorption isotherm of the composite and the corresponding pore size distribution. A mixed micro/mesoporous structure coexists in the pomegranate, with the micropores coming probably from the carbonization of sucrose with release of volatile species,[48] while the meso/macropores arise from the decomposition of nitrides during pyrolysis. The meso- and macropores in the pomegranate FeCo/LiF/C composite allow the liquid electrolyte to penetrate into FeCo/LiF/C spheres, accelerating the ion transport and accommodating the volume change of FeCo/LiF during the repeated lithiation/delithiation reactions. Meanwhile, the flexible and conductive carbon matrix with pores can inhibit the aggregation of FeCo nanoparticles and thus maintain the structural and electrical integrity of the FeCo/LiF/C electrode during the prolonged charging/discharging cycles. Closely similar structure was found for FeNi/LiF/C composites, as clearly shown in Figure S4. Therefore, it can be concluded that the present aerosol-spray pyrolysis approach provides a versatile method for other prelithiated TM fluorides.

Electrochemical Performance. The electrochemical performance of the pomegranate-like FeCo/LiF/C composite was studied by cyclic voltammetry (CV) and galvanostatic charge/discharge cycling in coin cells. Figure 5a shows the first four CV profiles at room temperature between 1.2 and 4.5 V at a scanning rate of 0.1 mV s^{-1}. Apparent difference is observed between the CVs of the first and the following cycles, especially for the charge process. The high peak current potential and low

DOI: 10.1021/acsnano.6b02309
ACS Nano 2016, 10, 5567−5577

initial current below 3.2 V in the first delithiation process demonstrates that a large driving force is needed to initiate the delithiation reaction in the FeCo/LiF/C composite.

In the subsequent delithiation, two large delithiation peaks around 3.0 and 3.4 V can be observed, which is probably attributed to conversion reaction from FeCo and LiF to Li_yFeCoF_x and then further delithiation to $FeCoF_x$ (or FeF_x and CoF_y). For the lithiation process, one shoulder at 3.2 V and two large peaks at 2.3 and 1.8 V were observed. The former can be ascribed to lithium insertion of trifluoride, forming Li_yFeF_3,[49] while the following two peaks may be associated with conversion reaction of Li_yFeCoF_x to FeCo and LiF.[33,40] The relatively large overpotential/hysteresis for the conversion reaction is related to the large energy barriers for the formation/dissociation of the LiF and the transport of the heavier ions during charging/discharging processes.[50,51] The peak intensity slightly increased during the initial four cycles, indicating that an activation process needed to extract most of the lithium from the prelithiated materials.

Figure 5b,c shows the representative charge/discharge profiles of FeCo/LiF/C cathodes between 1.2 and 4.5 V. In the first five cycles, a constant current/constant voltage (CCCV) charging algorithm followed by galvanostatic discharge was used to activate the lithiated (discharged) FeCo/LiF/C cathode (Figure 5a), which was delithiated (charged) at 30 mA/g to 4.5 V and then maintained at 4.4 V for 6 h to ensure the full delithiation, followed by discharging at a current of 30 mA g^{-1} down to 1.2 V. After activation, the FeCo/LiF/C cathode was galvanostatically cycled at 30 mA g^{-1} between 1.2 and 4.5 V (Figure 5c). Unlike intercalation-type cathode materials, where flat plateaus appear during Li^+ insertion into and extraction from the topotactic lattices, the FeCo/LiF/C nanocomposite presents rather sloppy profiles typical of conversion-reaction materials due to breaking of Li−F and formation of FeCo−F bonds. After activation, two plateaus appear at 3.5−2 and 2−1.2 V, respectively, in the discharge profile of the delithiated cathode (Figure 5c). The higher plateau may arise from the intercalation reaction of $FeCoF_x$ with Li^+, while the lower plateau should be associated with the conversion reaction of $LiFeCoF_x$ (or FeF_2 and CoF_2) into FeCo and LiF, which is in line with the CV curves. The electrode delivers an initial charge capacity of 261 mA h g^{-1}, which increases to 300 mA h g^{-1} after activation and remains at ∼300 mA h g^{-1} even after 100 cycles (Figure 5d). In stark contrast, the as-synthesized Fe/LiF/C composite exhibits only a capacity of ∼140 mA h g^{-1} (Figure S5) due to the formation of Fe_3C, which is electrochemically inactive to the lithiation/delithiation reactions. To our best knowledge, the pomegranate-like FeCo/LiF/C electrode is superior to all prelithiated metal fluorides synthesized *via* traditional pyrolysis[32,33,35,43] in terms of total capacity and cycling stability and even outperforms nanostructured nonlithiated FeF_3,[52,53] CoF_2,[54] FeF_3/C composites,[29,53,55] and CoF_2/C composites.[33,54] The pronounced improvement should be attributed to the unique pomegranate structure and morphology of the FeCo/LiF/C nanocomposite that offers the following benefits: (1) the *in situ* synthesized FeCo and LiF nanoparticles (both <20 nm), both uniformly embedded in the carbon matrix, ensure the intimate contact of the active species and the short diffusion paths for electrons, lithium, and fluorine ions; (2) the interconnected carbon matrix constructs a very efficient and continuous conductive network for electrons, lithium, and fluorine ions and circumvents the poor conductivity of metal fluorides; and (3) the FeM/LiF/C cathode nanocomposite with built-in Li source is already in an expended state, and the flexible carbon matrix with micropores can sufficiently absorb the volume change near FeM due to conversion of FeM to $FeMF_3$ (or FeF_x, MF_y), thus the pulverization of FeM/LiF/C is minimized due to the benefits of cycling stability.

The nature of the hysteresis between lithiation and delithiation of FeCo/LiF/C was also investigated by differentiating the thermodynamic potential hysteresis from kinetic polarization using a galvanostatic intermittent titration technique (GITT). During GITT measurements, the FeCo/LiF/C cathode was charged/discharged using a current pulse of 40 mA g^{-1} for a duration of 1 h. Following each pulse, the cathode will then be rested at open circuit for 20 h to reach equilibrium, as shown in Figure 5e, in which the hollow dots represent the equilibrium open-circuit potentials.

The complete GITT profiles, including the voltage relaxation process during the rest, are shown in Figure S6. In GITT, the gradual change in the potential should be attributed to the ion diffusion, while the sudden change is due to the charge transfer and ohm resistance. Figure S7 presents the enlargements of open-circuit relaxation curves at the beginning and end of charge/discharge, which clearly show that the diffusion resistance is small at the beginning of lithiation and delithiation but gradually increases upon lithiation or delithiation processes. Figure 5e reveals that the thermodynamic open-circuit potential after 50% lithiation or delithiation become very flat, demonstrating an obvious phase transformation process. The thermodynamic potential hysteresis is rather small at the beginning and end of charge/discharge but is about 700 mV in the phase transformation region. However, it is still substantially lower than that of nonlithiated FeF_2 (1.28 V).[56] This significant reduction in the hysteresis should be attributed to the extremely small particle sizes of the active species, their unique pomegranate-like arrangements, as well as the binary metal alloy. It has been reported that the substitution of cations can effectively suppress both overpotentials and hysteresis during charge/discharge cycling and improve the charge/discharge kinetics of the fluorides.[57]

The GITT curve also indicates that the FeCo/LiF/C composite can potentially provide a capacity of over 400 mA h g^{-1} with a discharge energy density of over 1100 Wh kg^{-1} if the charge and discharge rates are reduced. At a current of 40 mA g^{-1}, the kinetic reaction resistance takes more than two-thirds of the total resistance (thermodynamic potential hysteresis and overpotentials), and diffusion resistance becomes the major contributor of the overpotential after initial activation. Therefore, FeCo and LiF particle sizes play a critical role in defining the energy efficiency, with a plausible explanation that, for the conversion reaction chemistries, slow diffusion of the F^- ion or even Fe ions is the rate-determining step during the charging and discharging processes.

To confirm the formation of transition metal fluorides after FeCo/LiF/C is fully activated (delithiated), the phase structure of the fully charged FeCo/LiF/C was investigated using *ex situ* XRD and X-ray photoelectron spectroscopy (XPS). Figure 6a and Figure S8 show the XRD patterns for the FeCo/LiF/C composite after being charged to 4.5 V and kept at 4.4 V for 48 h. Several small broadened peaks (bumps) at 26.8, 33.1−34.3, and 51.8° can be indexed to the tetragonal FeF_2 (PDF# 45-1602) and CoF_2 (PDF# 33-1407). The broad bumps with low intensity reflected the small grain size for the formed transition metal fluorides after being charged to 4.5 V. $Fe_{0.5}Co_{0.5}F_3$ or

DOI: 10.1021/acsnano.6b02309
ACS Nano 2016, 10, 5567−5577

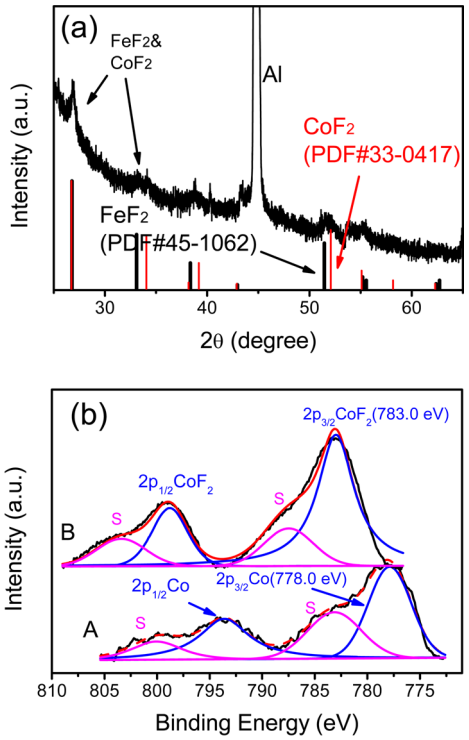

Figure 6. Characterization for the pomegranate-like nanocomposite electrode after the initial activation: (a) XRD pattern after being charged (delithiated) to 4.5 V after the fifth cycle and then kept at 4.4 V for 48 h. Also included as a comparison are the standard diffraction peaks for the FeF_2 (black lines) and CoF_2 (red lines). (b) Comparison of the narrow scan XPS spectra for the Co 2p in charged (B) and as-synthesized (A) electrodes. The blue peaks are the Co 2p peaks, and the magenta peaks are the satellite peaks, which are denoted as S in the figure.

FeF_3 phases were not detected in XRD; however, the potential plateau at the high discharge voltage region (4−2.2 V) in Figure 5b confirms the existence of $Fe_{0.5}Co_{0.5}F_3$ or FeF_3 phases. Therefore, $Fe_{0.5}Co_{0.5}F_3$ or FeF_3 phases should exist in extremely small particle sizes or even a distorted state.[13] The small grain size of FeF_3 after one full discharge/charge cycle was also reported for the nonlithiated FeF_3/C composite.[28,58] A small broad peak at 38.5° can be ascribed to the unreacted LiF species. The residual LiF phase indicates an incomplete conversion reaction of the composite and can explain why the capacities, especially for the high-voltage region during discharge, are less than what the full reaction of FeF_3 and CoF_2 should provide. Figure S9 shows the wide scan XPS results of charged and fresh FeCo/LiF/C electrodes, where all the related elements can be detected on the electrode surfaces. Since Fe 2p signals overlapped with F 1s, we characterized the Co 2p peaks instead, as shown in Figure 6b. It is found that the binding energy of Co 2p shifts from 778 eV to a higher level at ∼783 eV after activation, which should correspond to the formation of CoF_2.[59,60]

SEM and TEM were used to further characterize the morphology and structure of the cathode nanocomposite after its full activation at 4.5 V (Figure 7). After the fifth cycle, the FeCo/LiF/C composite still maintains the morphology of pristine composite spheres of pomegranate-like architecture (Figure 7a,b), demonstrating the robustness of this spherical nanostructure. TEM and HRTEM images (Figure 7c,d and Figure S10) with the electron energy loss spectra (Figure 7e−g) reveal the detailed structure and the elemental distribution of the fully charged nanocomposite. Compared with the pristine composite where the distinct FeCo and LiF (10−20 nm) nanoparticles are uniformly dispersed in the carbon matrix (Figure 4) as pomegranate-like seeds, much smaller nanoclusters (2−5 nm) with poor crystallinity (Figure 7d and Figure S10) were observed after five activation cycles, in good agreement with the extremely broadened XRD peaks for the electrode after cycling (Figure 6a). The aggregation of nanoclusters is in the size of 20−30 nm and uniformly dispersed in the composite electrode, indicating that these nanoclusters with a size of 2−5 nm are generated from the reaction of FeCo and F^- after the charge (delithiation) process. Figure 7e−g presents the distribution of Fe, Co, and F for the nanocomposite electrode after delithiation, with the EDS spectra shown as the inset in Figure 7h. The majority of F overlaps with Fe or Co areas. This is quite different from the pristine FeCo/LiF/C composite, where the F is totally separated from FeCo species while overlapping with carbon (Figure 4). The slow reaction kinetics prevented the conversion reaction from proceeding to completion, which accounts for the partial distribution deviation of the transition metals to that of F, as well as the capacity being smaller than the theoretical expectation for the FeCo/LiF/C nanocomposite.

Based on the electrochemical behavior and the corresponding structure/morphology changes observed, the conversion-reaction mechanism of the FeCo/LiF/C nanocomposite is proposed, as schematically illustrated in Figure 7i. The uniform dispersion and good connection of fresh FeCo and LiF nanoparticles within the conductive carbon matrix allows for an initial fast electron and ion transport for the delithiation of the pristine nanocomposite, in which the Li^+ ions were extracted from the LiF nanoparticles, with the F^- diffusing to the neighboring FeCo nanoparticles through carbon and producing the charged state of the $FeCoF_x$ cathode. This process is accompanied by large stress/strain and a high overpotential.

The overpotential was significantly reduced in the following cycles due to the relaxation of stress and reduction of FeCo particle size from ∼10 to 2−5 nm. In the following lithiation processes, these small metal fluoride nanoparticles transformed to the small transition metal clusters of FeCo and LiF nanoparticles. The small particle size and large interfacial area among the active species within the pomegranate-like nanocomposites allowed for fast charge transfer and short ion transport length, resulting in a fast and reversible conversion reaction chemistry with superior electrochemical performances observed thus far for any conversion-reaction cathode materials.

CONCLUSION

We designed and synthesized a prelithiated conversion-reaction material, FeM/LiF/C (M = Co, Ni), *via* a scalable and continuous aerosol-spray pyrolysis approach, in which primary LiF nanoparticles (∼20 nm) and FeM nanoparticles (∼10 nm in diameter) coated with uniform graphene layers (2−3 nm in thickness) are arranged as distinct pomegranate-like seeds within a carbonaceous secondary microsphere. This unique nanoarchitecture provides shortened ion diffusion distance, intimate contacts among the active FeCo and LiF species, good electronic conductivity of the carbon matrix, and superior structure robustness against strain and stress induced by the repeated bond-breaking and re-formation. The as-synthesized ternary nanocomposite FeCo/LiF/C exhibits a reversibility with a high capacity of ∼300 mA h g^{-1} at 1.2−4.5 V for over

DOI: 10.1021/acsnano.6b02309
ACS Nano 2016, 10, 5567−5577

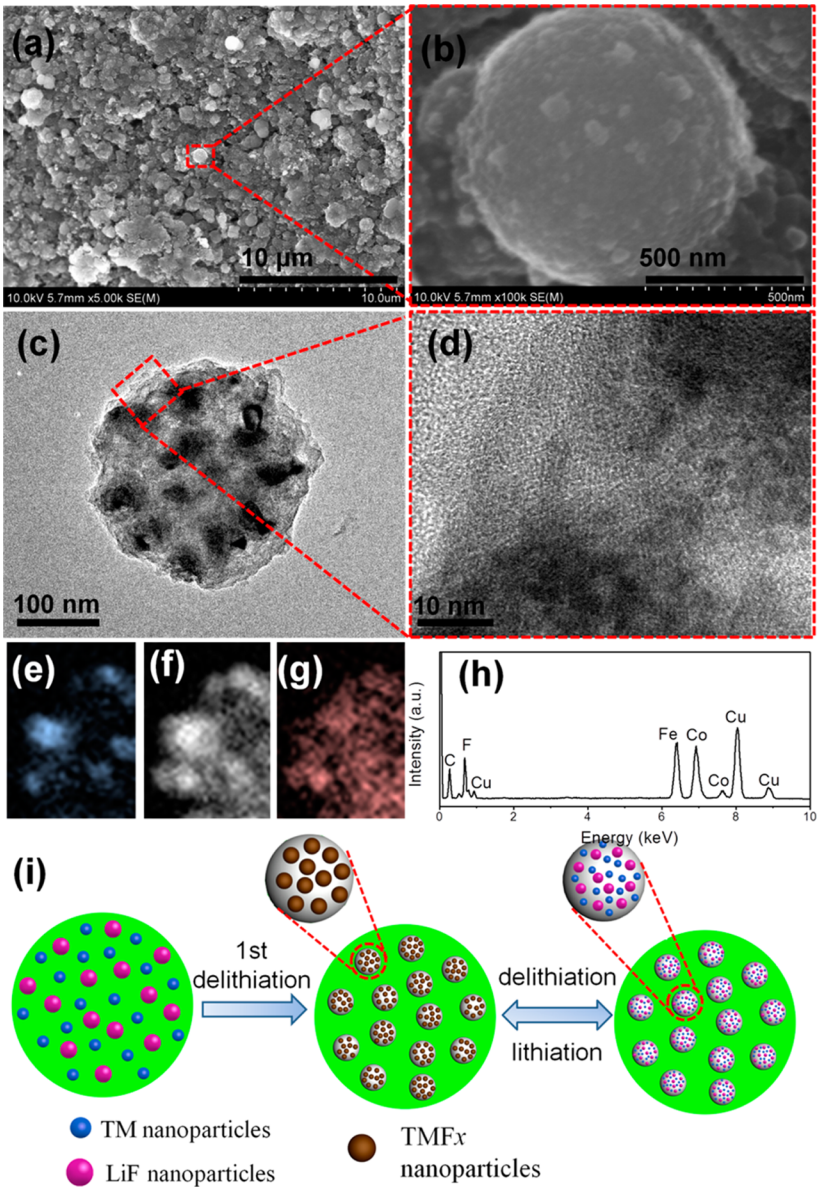

Figure 7. SEM (a,b), TEM (c), and HRTEM (d) images of the pomegranate-like nanocomposite electrode charged to 4.5 V after the fifth cycle, then kept at 4.4 V for 48 h. (e–g) Electron energy loss spectra of Co, Fe, and F recorded for the area shown in (c). (h) Corresponding EDS results of (c). (i) Schematic illustration of cycling effects on the microstructure evolvement of the FeCo/LiF/C sphere electrode.

100 cycles, which is one of the best prelithiated metal fluoride cathodes ever reported for the conversion-reaction material. The present *in situ* and high-yield strategy for the synthesis of pomegranate FeCo/LiF/C composites can be extended to construct a variety of other prelithiated materials based on fluorides, sulfides, and oxyfluorides of important interest for applications in high-performance LIBs.

EXPERIMENTAL SECTION

Synthesis of the FeCo/LiF/C Composite. FeCo/LiF/C composite spheres were synthesized by aerosol-spray pyrolysis. $Fe(NO_3)_3{\cdot}9H_2O$ (1.818 g, 0.0045 mol), $Co(NO_3)_2{\cdot}6H_2O$ (1.31 g, 0.0045 mol), NH_4F (0.833 g, 0.0225 mol), $CH_3COOLi{\cdot}2H_2O$ (2.3 g, 0.0225 mol), sucrose (3.5 g), and nitric acid (3 mL, 70%) were dissolved into 90 mL of water. The molar ratio of Fe, Co, and LiF is 1:1:5, assuming that FeF_3 and CoF_2 can be obtained after full delithiation. The solution was atomized by argon/5% hydrogen flow with a collision-type nebulizer (Atomizer Aerosol Generator ATM 220, TOPAS, Germany), and the aerosols that were generated subsequently entered a tubular furnace at 750 °C. The flow rate of the precursor solution vapor was 200 $cm^3\ s^{-1}$. The diameter of the tube furnace was 2.54 cm, and the heating length was 40 cm. The residential time of the pyrolysis reaction was calculated to be ~1 s based on the following equation:

$$\text{residue time} = \frac{\pi \times (\text{radius of tube furnace})^2 \times \text{heating length}}{\text{flow rate}} \quad (2)$$

During that time, the Fe and Co will be reduced with LiF generation, and carbon formation will be catalyzed by Fe and Co from sucrose, yielding the FeCo/LiF/C composite spheres. The overall reaction will be

$$\begin{aligned} &2Fe(NO_3)_3 + 2Co(NO_3)_2 + 10NH_4F + 10CH_3COOLi \\ &\quad + HNO_3 + C_{12}H_{22}O_{11} \\ &\rightarrow 2FeCo + 10LiF + 12C + 20CO\uparrow + 9.5H_2\uparrow + 22H_2O\uparrow \\ &\quad + 11NO_2\uparrow + 10NH_3\uparrow \end{aligned} \quad (3)$$

DOI: 10.1021/acsnano.6b02309
ACS Nano 2016, 10, 5567–5577

The final dark product was collected on a 200 nm (pore size) DTTP Millipore filter. Fe/LiF/C and FeNi/LiF/C composites were synthesized using the same procedures as used for the FeCo/LiF/C composite.

Material Characterizations. Scanning electron microscopy and transmission electron microscopy images were taken by a Hitachi SU-70 analytical SEM (Japan) and JEOL (Japan) 2100F field emission TEM, respectively. The XRD pattern was recorded by Bruker Smart 1000 (Bruker AXS Inc., USA) using Cu Kα radiation. Raman measurements were performed on a Horiba Jobin Yvon Labram Aramis using a 532 nm diode-pumped solid-state laser, attenuated to give ~900 μW power at the sample surface. Thermogravimetric analysis and differential scanning calorimetry was carried out using a Netzsch STA 449F3 (Germany) in air at a heating rate of 3 °C/min. Specific surface area for the sample was characterized with N_2 adsorption by means of a Quantachrome Autosorb-1-C system using the Brunauer–Emmett–Teller method. X-ray photoelectron spectroscopy was conducted on a high-sensitivity Kratos AXIS 165 X-ray photoelectron spectrometer with Mg Kα radiation. All binding energy values were referenced to the C 1s peak of carbon at 284.6 eV.

Electrochemical Measurements. The electrochemical tests were performed using a coin-type half-cell (CR 2032) with metallic lithium as the negative electrode. To prepare the working electrode, the as-synthesized FeCo/LiF/C spherical composite, carbon black, and PVDF with a mass ratio 70:15:15 were mixed into a homogeneous slurry in NMP with pestle and mortar. The slurry mixture was coated onto Al foil and then dried at 100 °C for 12 h under an Ar atmosphere. The loading mass of the active materials for the electrode was about 0.2 mg/cm^2. The electrode contained FeCo and LiF nanoparticles with an average diameter of <20 nm. These extremely small and uniform FeCo nanoparticles served as very active catalysts for the decomposition reaction of the solvents (such as EC or DMC) above 3.5 V during the first charging process. Therefore, electrolytes based on fluorinated solvents with high voltage stability have to be used to suppress the oxidative decompositions during the charging process.[61,62] The electrolyte solution comprised saturated $LiPF_6$ in fluoroethylene carbonate/2,2,2-trifluoroethyl methyl carbonate/hydrofluoroether (2:6:2 by volume). The cells were assembled with a polypropylene microporous film (Celgard 3501) as the separator. Electrochemical performance was tested using an Arbin battery test station (BT2000, Arbin Instruments, USA). Capacity was calculated on the basis of the active mass. A cyclic voltammogram scanned at 0.1 mV/s between 1.2 and 4.5 V was recorded using a CHI 600E electrochemical workstation (CH Instruments Inc. USA).

ASSOCIATED CONTENT

Supporting Information

The Supporting Information is available free of charge on the ACS Publications website at DOI: 10.1021/acsnano.6b02309.

Figures S1–S10 (PDF)

AUTHOR INFORMATION

Corresponding Authors

*E-mail: conrad.k.xu.civ@mail.mil.

*E-mail: cswang@umd.edu.

Notes

The authors declare no competing financial interest.

ACKNOWLEDGMENTS

This work was supported by the Army Research Lab under Award Number W911NF1420031. The authors gratefully acknowledge the support of the Maryland NanoCenter and its NispLab. The highly pure fluorinated solvents were provided by Drs. Ron Hendershot and Joe Sundstrom of Daikin America.

REFERENCES

(1) Ellis, B. L.; Lee, K. T.; Nazar, L. F. Positive Electrode Materials for Li-Ion and Li-Batteries. *Chem. Mater.* **2010**, *22*, 691–714.

(2) Etacheri, V.; Marom, R.; Elazari, R.; Salitra, G.; Aurbach, D. Challenges in the Development of Advanced Li-Ion Batteries: a Review. *Energy Environ. Sci.* **2011**, *4*, 3243–3262.

(3) Whittingham, M. S. Ultimate Limits to Intercalation Reactions for Lithium Batteries. *Chem. Rev.* **2014**, *114*, 11414–11443.

(4) Bruce, P. G.; Freunberger, S. A.; Hardwick, L. J.; Tarascon, J. M. Li-O_2 and Li-S Batteries with High Energy Storage. *Nat. Mater.* **2012**, *11*, 19–29.

(5) Park, C. M.; Kim, J. H.; Kim, H.; Sohn, H. J. Li-Alloy Based Anode Materials for Li Secondary Batteries. *Chem. Soc. Rev.* **2010**, *39*, 3115–3141.

(6) Kasavajjula, U.; Wang, C.; Appleby, A. J. Nano- and Bulk-Silicon-Based Insertion Anodes for Lithium-Ion Secondary Cells. *J. Power Sources* **2007**, *163*, 1003–1039.

(7) Son, S. B.; Yersak, T. A.; Piper, D. M.; Kim, S. C.; Kang, C. S.; Cho, J. S.; Suh, S. S.; Kim, Y. U.; Oh, K. H.; Lee, S. H. A Stablized PAN-FeS_2 Cathode with an EC/DEC Liquid Electrolyte. *Adv. Energy Mater.* **2014**, *4*, 1300961.

(8) Sun, Y.; Lee, H. W.; Zheng, G.; Seh, Z. W.; Sun, J.; Li, Y.; Cui, Y. *In situ* Chemical Synthesis of Lithium Fluoride/Metal Nanocomposite for High Capacity Prelithiation of Cathodes. *Nano Lett.* **2016**, *16*, 1497–1501.

(9) Liu, J.; Wen, Y.; Wang, Y.; van Aken, P. A.; Maier, J.; Yu, Y. Carbon-Encapsulated Pyrite as Stable and Earth Abundant High Energy Cathode Material for Rechargeable Lithium Batteries. *Adv. Mater.* **2014**, *26*, 6025–6030.

(10) Reddy, M. A.; Breitung, B.; Chakravadhanula, V. S. K.; Wall, C.; Engel, M.; Kübel, C.; Powell, A. K.; Hahn, H.; Fichtner, M. CF_x Derived Carbon-FeF_2 Nanocomposites for Reversible Lithium Storage. *Adv. Energy Mater.* **2013**, *3*, 308–313.

(11) Gu, W.; Magasinski, A.; Zdyrko, B.; Yushin, G. Metal Fluorides Nanoconfined in Carbon Nanopores as Reversible High Capacity Cathodes for Li and Li-Ion Rechargeable Batteries: FeF_2 as an Example. *Adv. Energy Mater.* **2015**, *5*, 1401148.

(12) Yamakawa, N.; Jiang, M.; Grey, C. P. Investigation of the Conversion Reaction Mechanisms for Binary Copper (II) Compounds by Solid-State NMR Spectroscopy and X-Ray Diffraction. *Chem. Mater.* **2009**, *21*, 3162–3176.

(13) Doe, R. E.; Persson, K. A.; Meng, Y. S.; Ceder, G. First-Principles Investigation of the Li-Fe-F Phase Diagram and Equilibrium and Nonequilibrium Conversion Reactions of Iron Fluorides with Lithium. *Chem. Mater.* **2008**, *20*, 5274–5283.

(14) Li, H.; Richter, G.; Maier, J. Reversible Formation and Decomposition of LiF Clusters Using Transition Metal Fluorides as Precursors and Their Application in Rechargeable Li Batteries. *Adv. Mater.* **2003**, *15*, 736–739.

(15) Andre, D.; Kim, S. J.; Lamp, P.; Lux, S. F.; Maglia, F.; Paschos, O.; Stiaszny, B. Future Generations of Cathode Materials: an Automotive Industry Perspective. *J. Mater. Chem. A* **2015**, *3*, 6709–6732.

(16) Amatucci, G. G.; Pereira, N. Fluoride Based Electrode Materials for Advanced Energy Storage Devices. *J. Fluorine Chem.* **2007**, *128*, 243–262.

(17) Arai, H.; Okada, S.; Sakurai, Y.; Yamaki, J. I. Cathode Performance and Voltage Estimation of Metal Trihalides. *J. Power Sources* **1997**, *68*, 716–719.

(18) Wang, F.; Robert, R.; Chernova, N. A.; Pereira, N.; Omenya, F.; Badway, F.; Hua, X.; Ruotolo, M.; Zhang, R.; Wu, L.; Volkov, V.; Su, D.; Key, B.; Whittingham, M. S.; Grey, C. P.; Amatucci, G. G.; Zhu, Y.; Graetz, J. Conversion Reaction Mechanisms in Lithium Ion Batteries: Study of the Binary Metal Fluoride Electrodes. *J. Am. Chem. Soc.* **2011**, *133*, 18828–18836.

(19) Yamakawa; Jiang, N. M.; Key, B.; Grey, C. P. Identifying the Local Structures Formed during Lithiation of the Conversion Material, Iron Fluoride, in a Li Ion Battery: a Solid-State NMR, X-Ray

DOI: 10.1021/acsnano.6b02309
ACS Nano 2016, 10, 5567–5577

Diffraction, and Pair Distribution Function Analysis Study. *J. Am. Chem. Soc.* **2009**, *131*, 10525−10536.
(20) Liu, L.; Zhou, M.; Yi, L.; Guo, H.; Tan, J.; Shu, H.; Yang, X.; Yang, Z.; Wang, X. Excellent Cycle Performance of Co-Doped FeF_3/C Nanocomposite Cathode Material for Lithium-Ion Batteries. *J. Mater. Chem.* **2012**, *22*, 17539−17550.
(21) Kim, S. W.; Seo, D. H.; Gwon, H.; Kim, J.; Kang, K. Fabrication of FeF_3 Nanoflowers on CNT Branches and Their Application to High Power Lithium Rechargeable Batteries. *Adv. Mater.* **2010**, *22*, 5260−5264.
(22) Liu, J.; Liu, W.; Ji, S.; Wan, Y.; Gu, M.; Yin, H.; Zhou, Y. Iron Fluoride Hollow Porous Microspheres: Facile Solution-Phase Synthesis and Their Application for Li-Ion Battery Cathodes. *Chem. - Eur. J.* **2014**, *20*, 5815−5820.
(23) Li, C.; Mu, X.; van Aken, P. A.; Maier, J. High-Capacity Cathode for Lithium Batteries Consisting of Porous Microspheres of Highly Amorphized Iron Fluoride Densified from Its Open Parent Phase. *Adv. Energy Mater.* **2013**, *3*, 113−119.
(24) Lu, Y.; Wen, Z. Y.; Jin, J.; Wu, X. W.; Rui, K. Size-Controlled Synthesis of Hierarchical Nanoporous Iron Based Fluorides and Their High Performances in Rechargeable Lithium Ion Batteries. *Chem. Commun.* **2014**, *50*, 6487−6490.
(25) Li, C.; Gu, L.; Tong, J.; Tsukimoto, S.; Maier, J. Mesoporous Iron-Based Fluoride Cathode of Tunnle Structure for Rechargeable Lithium Batteries. *Adv. Funct. Mater.* **2011**, *21*, 1391−1397.
(26) Makimura, Y.; Rougier, A.; Tarascon, J. M. Pulsed Laser Deposited Iron Fluoride Thin Films for Lithium-Ion Batteries. *Appl. Surf. Sci.* **2006**, *252*, 4587−4592.
(27) Makimura, Y.; Rougier, A.; Laffont, L.; Womes, M.; Jumas, J. C.; Leriche, J. B.; Tarascon, J. M. Electrochemical Behaviour of Low Temperature Grown Iron Fluoride Thin Films. *Electrochem. Commun.* **2006**, *8*, 1769−1774.
(28) Badway, F.; Cosandey, F.; Pereira, N.; Amatucci, G. G. Carbon Metal Fluoride Nanocomposites: High-Capacity Reversible Metal Fluoride Conversion Materials as Rechargeable Positive Electrodes for Li Batteries. *J. Electrochem. Soc.* **2003**, *150*, A1318−A1327.
(29) Tan, H. J.; Smith, H. L.; Kim, L.; Harding, T. K.; Jones, S. C.; Fultz, B. Electrochemical Cycling and Lithium Insertion in Nanostructured FeF_3 Cathodes. *J. Electrochem. Soc.* **2014**, *161*, A445−A449.
(30) Zhang, S.; Lu, Y.; Xu, G.; Li, Y.; Zhang, X. LiF/Fe/C Nanofibres as a High-Capacity Cathode Material for Li-Ion Batteries. *J. Phys. D: Appl. Phys.* **2012**, *45*, 395301.
(31) Fan, X.; Shao, J.; Xiao, X.; Wang, X.; Li, S.; Ge, H.; Chen, L. $SnLi_{4.4}$ Nanoparticles Encapsulated in Carbon Matrix as High Performance Anode Material for Lithium-Ion Batteries. *Nano Energy* **2014**, *9*, 196−203.
(32) Prakash, R.; Mishra, A. K.; Roth, A.; Kubel, C.; Scherer, T.; Ghafari, M.; Hahn, H.; Fichtner, M. A Ferrocence-Based Carbon-Iron Lithium Fluoride Nanocomposite as a Stable Electrode Material in Lithium Batteries. *J. Mater. Chem.* **2010**, *20*, 1871−1876.
(33) Wall, C.; Prakash, R.; Kübel, C.; Hahn, H.; Fichtner, M. Synthesis of [Co/LiF/C] Nanocomposite and Its Application as Cathode in Lithium-Ion Batteries. *J. Alloys Compd.* **2012**, *530*, 121−126.
(34) Ma, R.; Dong, Y.; Xi, L.; Yang, S.; Lu, Z.; Chung, C. Fabrication of LiF/Fe/Graphene Nanocomposites as Cathode Material for Lithium-Ion Batteries. *ACS Appl. Mater. Interfaces* **2013**, *5*, 892−897.
(35) Zhou, Y.; Wu, C.; Zhang, H.; Wu, X.; Fu, Z. The Electrochemical Properties of LiF-Ni Nanocomposite Thin Film. *Acta Phys. Chim. Sin.* **2006**, *22*, 1111−1115.
(36) Yu, X. Q.; Sun, J. P.; Tang, K.; Li, H.; Huang, X. J.; Dupont, L.; Maier, J. Reversible Lithium Storage in LiF/Ti Nanocomposites. *Phys. Chem. Chem. Phys.* **2009**, *11*, 9497−9503.
(37) Poizot, P.; Laruelle, S.; Grugeon, S.; Dupont, L.; Tarascon, J. M. Nano-Sized Transition-Metal Oxides as Negative-Electrode Materials for Lithium-Ion Batteries. *Nature* **2000**, *407*, 496−499.
(38) Rui, K.; Wen, Z.; Lu, Y.; Jin, J.; Shen, C. One-Step Solvothermal Synthesis of Nanostructured Manganese Fluoride as an Anode for Rechargeable Lithium-Ion Batteries and Insights into the Conversion Mechanism. *Adv. Energy Mater.* **2015**, *5*, 1401716.
(39) Yersak, T. A.; Macpherson, H. A.; Kim, S. C.; Le, V. D.; Kang, C. S.; Son, S. B.; Kim, Y. H.; Trevey, J. E.; Oh, K. H.; Stoldt, C.; Lee, S. H. Solid State Enabled Reversible Four Electron Storage. *Adv. Energy Mater.* **2013**, *3*, 120−127.
(40) Li, H.; Balaya, P.; Maier, J. Li-Storage *via* Heterogeneous Reaction in Selected Binary Metal Fluorides and Oxides. *J. Electrochem. Soc.* **2004**, *151*, A1878−A1885.
(41) Liao, P.; Li, J.; Dahn, J. R. Lithium Intercalation in $LiFe_2F_6$ and $LiMgFeF_6$ Disordered Trirutile-Type Phases. *J. Electrochem. Soc.* **2010**, *157*, A355−A361.
(42) Sunkara, B.; Zhan, J.; Kolesnichenko, I.; Wang, Y.; He, J.; Holland, J. E.; McPherson, G. L.; John, V. T. Modifying Metal Nanoparticle Placement on Carbon Supports Using an Aerosol-Based Process, with Application to the Environmental Remediation of Chlorinated Hydrocarbons. *Langmuir* **2011**, *27*, 7854−7859.
(43) Prakash, R.; Wall, C.; Mishra, A. K.; Kübel, C.; Ghafari, M.; Hahn, H.; Fichtner, M. Modified Synthesis of [Fe/LiF/C] Nanocomposite, and Its Application as Conversion Cathode Material in Lithium Batteries. *J. Power Sources* **2011**, *196*, 5936−5944.
(44) He, C.; Wu, S.; Zhao, N.; Shi, C.; Liu, E.; Li, J. Carbon-Encapsulated Fe_3O_4 Nanoparticles as a High-Rate Lithium Ion Battery Anode Material. *ACS Nano* **2013**, *7*, 4459−4469.
(45) Zhou, J.; Qian, T.; Yang, T.; Wang, M.; Guo, J.; Yan, C. Nanomeshes of Highly Crystalline Nitrogen-Doped Carbon Encapsulated Fe/Fe_3C Electrodes as Ultrafast and Stable Anodes for Li-Ion Batteries. *J. Mater. Chem. A* **2015**, *3*, 15008−15014.
(46) Portnoi, V. K.; Leonov, A. V.; Mudretsova, S. N.; Fedotov, S. A. Formation of Nickel Carbide in the Course of Deformation Treatment of Ni-C Mixtures. *Phys. Met. Metallogr.* **2010**, *109*, 153−161.
(47) Tanaka, T.; Ishihara, K. N.; Shingu, P. H. Formation of Metastable Phases of Ni-C. *Metall. Mater. Trans. A* **1992**, *23*, 2431−2435.
(48) Parmentier, J.; Saadhallah, S.; Reda, M.; Gibot, P.; Roux, M.; Vidal, L.; Vix-Guterl, C.; Patarin, J. New Carbons with Controlled Nanoporosity Obtained by Nanocasting Using a SBA-15 Mesoporous Silica Host Matrix and Different Preparation Routes. *J. Phys. Chem. Solids* **2004**, *65*, 139−146.
(49) Ma, D.; Cao, Z.; Wang, H.; Huang, X.; Wang, L.; Zhang, X. Three-Dimensionally Ordered Macroporous FeF_3 and Its *in situ* Homogenous Polymerization Coating for High Energy and Power Density Lithium Ion Batteries. *Energy Environ. Sci.* **2012**, *5*, 8538−8542.
(50) Liu, P.; Vajo, J. J.; Wang, J. S.; Li, W.; Liu, J. Thermodynamics and Kinetics of the Li/FeF_3 Reaction by Electrochemical Analysis. *J. Phys. Chem. C* **2012**, *116*, 6467−6473.
(51) Wang, F.; Yu, H. C.; Chen, M. H.; Wu, L.; Pereira, N.; Thornton, K.; Van der Ven, A.; Zhu, Y.; Amatucci, G. G.; Graetz, J. Tracking Lithium Transport and Electrochemical Reactions in Nanoparticles. *Nat. Commun.* **2012**, *3*, 1201.
(52) Li, L.; Meng, F.; Jin, S. High-Capacity Lithium-Ion Battery Conversion Cathodes Based on Iron Fluoride Nanowires and Insights into the Conversion Mechanism. *Nano Lett.* **2012**, *12*, 6030−6037.
(53) Zhao, X.; Hayner, C. M.; Kung, M. C.; Kung, H. H. Photothermal-Assisted Fabrication of Iron Fluoride-Graphene Composite Paper Cathodes for High-Energy Lithium-Ion Batteries. *Chem. Commun.* **2012**, *48*, 9909−9911.
(54) Armstrong, M. J.; Panneerselvam, A.; O'Regan, C.; Morris, M. A.; Holmes, J. D. Supercritical-Fluid Synthesis of FeF_2 and CoF_2 Li-Ion Conversion Materials. *J. Mater. Chem. A* **2013**, *1*, 10667−10676.
(55) Ma, R.; Wang, M.; Tao, P.; Wang, Y.; Cao, C.; Shan, G.; Yang, S.; Xi, L.; Chung, J. C. Y.; Lu, Z. Fabrication of FeF_3 Nanocrystals Dispersed into a Porous Carbon Matrix as a High Performance Cathode Material for Lithium Ion Batteries. *J. Mater. Chem. A* **2013**, *1*, 15060−15067.
(56) Ko, J. K.; Wiaderek, K. M.; Pereira, N.; Kinnibrugh, T. L.; Kim, J. R.; Chupas, P. J.; Chapman, K. W.; Amatucci, G. G. Transport, Phase Reactions, and Hysteresis of Iron Fluoride and Oxyfluoride

DOI: 10.1021/acsnano.6b02309
ACS Nano 2016, 10, 5567−5577

Conversion Electrode Materials for Lithium Batteries. *ACS Appl. Mater. Interfaces* **2014**, *6*, 10858−10869.
(57) Wang, F.; Kim, S.-W.; Seo, D.-H.; Kang, K.; Wang, L.; Su, D.; Vajo, J. J.; Wang, J.; Graetz, J. Ternary Metal Fluorides as High-Energy Cathodes with Low Cycling Hysteresis. *Nat. Commun.* **2015**, *6*, 6668.
(58) Cosandey, F.; Al-Sharab, J. F.; Badway, F.; Amatucci, G. G.; Stadelmann, P. EELS Spectroscopy of Iron Fluorides and FeF_x/C Nanocomposite Electrodes Used in Li-Ion Batteries. *Microsc. Microanal.* **2007**, *13*, 87−95.
(59) Jeon, S. H.; Kim, Y. S.; Jung, C. H. Cold Plasma Processing and Plasma Chemistry of Metallic Cobalt Surface. *Plasma Chem. Plasma Process.* **2008**, *28*, 617−628.
(60) Teng, Y. T.; Pramana, S. S.; Ding, J.; Wu, T.; Yazami, R. Investigation of the Conversion Mechanism of Nanosized CoF_2. *Electrochim. Acta* **2013**, *107*, 301−312.
(61) Fan, X.; Zhu, Y.; Luo, C.; Gao, T.; Suo, L.; Liou, S. C.; Xu, K.; Wang, C. *In situ* Lithiated FeF_3/C Nanocomposite as High Energy Conversion-Reaction Cathode for Lithium-Ion Batteries. *J. Power Sources* **2016**, *307*, 435−442.
(62) Read, J. A.; Cresce, A. V.; Ervin, M. H.; Xu, K. Dual-Graphite Chemistry Enabled by a High Voltage Electrolyte. *Energy Environ. Sci.* **2014**, *7*, 617−620.

DOI: 10.1021/acsnano.6b02309
ACS Nano 2016, 10, 5567−5577